Advances in Science and Technology Research Journal

Advances in Science and Technology Research Journal, 2025, 19(9), 317–332
https://doi.org/10.12913/22998624/207679
ISSN 2299-8624, License CC-BY 4.0

Received: 2025.05.12
Accepted: 2025.07.15
Published: 2025.08.01

Assessing energy efficiency and the application of artificial neural networks in wearable sensors using electrical impedance tomography

Mariusz Mazurek[1*], Marcin Dziadosz[2], Tomasz Rymarczyk[3,4], Dariusz Wójcik[3,4], Michalina Gryniewicz-Jaworska[3], Jolanta Słoniec[2]

[1] Institute of Philosophy and Sociology of the Polish Academy of Science, ul. Nowy Świat 72, 00-330 Warsaw, Poland
[2] Lublin University of Technology, ul. Nadbystrzycka 38D, 20-618 Lublin, Poland
[3] WSEI University, ul. Projektowa 4, 20-209 Lublin, Poland
[4] Research & Development Centre Netrix S.A., ul. Związkowa 26, 20-704 Lublin, Poland
* Corresponding author's e-mail: mmazurek@ifispan.edu.pl

ABSTRACT

Electrical impedance tomography (EIT) is a non-invasive imaging technique increasingly applied in biomedical diagnostics. Traditionally, EIT systems are stationary and require specialist knowledge to operate and interpret results. This study presents the development and evaluation of an innovative wearable EIT device designed for real-time monitoring of bladder function. The system enables visualization of bladder filling levels and is intended to support patients suffering from lower urinary tract dysfunctions. The device is designed for future integration with a mobile application that will inform users about urinary incontinence episodes and bladder status. A key component of the system is the implementation of an image reconstruction framework based on machine learning algorithms. Three models were evaluated – decision tree, elastic net, and a neural network (NNET) – with a focus on optimizing accuracy, computational efficiency, and energy consumption. The results demonstrate that the NNET model offers superior reconstruction quality and the lowest prediction time, making it the most suitable for wearable medical applications. The proposed solution is based on a process model incorporating an optimization procedure essential for device control and energy-efficient operation.

Keywords: energy efficiency, optimization, quality of experience, electrical impedance tomography, sensors, image reconstruction, non-invasive medical monitoring.

INTRODUCTION

This research aims to develop a sophisticated data reconstruction and measurement system, using electrical impedance tomography (EIT) and, eventually, ultrasound transmission tomography (UST) [1-9]. The primary objective is to incorporate this system into wearable technology, enabling non-invasive monitoring and diagnosis of functional urinary tract disorders in children.

Functional disorders of the urinary tract are common in the pediatric population, with studies indicating that over 20% of children under five years old and 2–4% of adolescents are affected. These conditions may occur alongside other anomalies in the urinary system, constipation, or neurological issues like spina bifida and cerebral palsy. However, many children experience these disorders independently, without associated health complications [3–4, 10].

The absence of non-invasive diagnostic tools for thorough functional assessment of the urinary tract hinders the ability to make accurate diagnoses and provide effective treatments. This gap may also lead to more children undergoing unnecessary treatments without clear clinical justification. Additionally, the development of a physical tomographic model is challenging due

to the intricate nature of acoustic wave behavior in small, heterogeneous environments within the body. Despite these challenges, the radial wave propagation model employed in UST has proven effective in identifying internal irregularities and is already used in medical practice for non-invasive diagnosis and monitoring of lower urinary tract dysfunctions. The innovative aspect of this approach lies in the combined evaluation of urinary tract function through the integration of Electrical Impedance Tomography and Ultrasound Tomography [3, 9].

EIT is a non-invasive imaging technology that allows visualization of internal body structures, including muscles, blood vessels, and organs. However, no EIT-based diagnostic system for the urinary tract is currently available globally. The development of such a system faces numerous hurdles, including limited research in the field, anatomical variations among individuals, and challenges in imaging bone structures and gas-filled areas. The envisioned system is intended for clinical use, where it will support the diagnosis of urinary tract dysfunctions in specific groups of children with confirmed disorders.

Innovation of solution

Diagnosis of urinary disorders in children is usually associated with a great deal of stress for the patient. Currently used objective diagnostic methods (e.g., complete urodynamic examination, which involves the insertion of a catheter into the bladder and a rectal probe to assess urinary tract function during bladder filling and during micturition) in most cases are characterized by a significant degree of invasiveness, which often leads to their results being burdened with numerous artifacts, often resulting in their misinterpretation. Therefore, the authors of the project decided to create a device for non-invasive urinary tract diagnostics, which will provide reliable results and significantly reduce negative feelings and risks for children with micturition disorders.

The device is ultimately intended to be a compilation of urinary potentials using electrical impedance tomography ultrasound and electromyography (EMG) for reading sphincter muscle tension (urethra and rectum). The energy efficiency of the device for the first method is currently being analysed. In the following stages, the full device will be studied. The device produced is expected to create the conditions for broader imaging diagnostics of urinary tract function without invasive techniques, reducing the stress and risk associated with this and expanding the range of methods and their availability to children. The child's participation in the study poses no additional health risks to the child related to the study procedures. The procedures will be carried out according to standards. The only difference is the combination of multiple consultations and activities into a single inpatient or outpatient visit. The benefit to the child will be a thorough medical specialty (urology) examination, a more thorough ultrasound evaluation of the urinary tract, and more detailed specialized advice (urologist/nephrologist and physiotherapist) on urinary hygiene conducted at the time of qualification for the study. The direct benefits of the proposed medical examinations will benefit children, who will be diagnosed more accurately and qualified for targeted diagnostics during the comprehensive evaluation. The advantage will be the comprehensiveness and reduced time spent performing three specialized visits simultaneously (usg/urologist/physiotherapist).

Children without urinary tract disorders will benefit from the test in the form of a more accurate evaluation of the urinary tract, urological consultation and specialized advice on urinary hygiene. The outcome of the entire project (the manufacture of a device for non-invasive urinary tract diagnosis) will benefit society by obtaining a non-invasive diagnostic tool – it is expected to reduce the suffering associated with lower urinary tract diagnosis.

Electrical impedance tomography for urological applications

Using EIT as a non-invasive method for assessing urinary tract function and the effects of urinary tract rehabilitation treatment is a unique solution on a global scale [1–2, 4]. There are no available urological diagnostic solutions of this type. The developed system will allow for continuous, long-term assessment of the current condition of the urinary tract. EIT is a technique sensitive to interference and requires the design of dedicated measurement sensors to ensure proper (electrical) contact with the patient's body [4, 11].

Based on the collected test results, the system will be designed to support the process of diagnosing urological diseases and planning individual therapy and rehabilitation dedicated to

a specific patient. The developed system is intended to be a tool supporting the doctor's work. The system will work based on measurement data from the device developed in the project and other diagnostic methods. Particular challenges when building such a system are: the development and implementation of deep neural network learning algorithms and the expansion of the classic approach to deep networks with elements of fuzzy set theory and fuzzy logic (deep neural fuzzy network), which will allow for the possible extension of the developed system with the possibility of interpreting the results of processes teaching and/or introducing additional, not necessarily precise, knowledge in the learning process. The authors believe that such a system will contribute to developing a reference method in treating urinary incontinence. They may influence guidelines in the diagnosis of functional urinary disorders. Currently, similar solutions are not available on the market [5–7].

Electrical impedance tomography

EIT includes ECT for systems dominated by dielectric materials and ERT for processes involving conductive materials. Although these sub-modalities require different hardware setups, the core theoretical basis for solving electrical tomography problems originates from Maxwell's equations [12–13]. Electrical tomography is an imaging technique that utilizes the varying electrical properties of materials. This method applies a voltage or current source to the object of interest, with measurements taken along its boundary. The acquired data is then processed by an algorithm that reconstructs the image [6, 8].

In ECT, measurements are obtained by assessing the capacitance between sensors positioned along the object's boundary, functioning as capacitor sensors. Electrical resistivity (or impedance) tomography similarly utilizes the varying electrical characteristics of materials for imaging. This method applies a voltage or energy source to the object, generating current flow or voltage distributions along its edges. The resulting data are processed through an algorithm that reconstructs the image. A key limitation of this tomography lies in its relatively low spatial resolution, primarily due to the restricted number of available measurements, the non-linear nature of current flow through the medium, and the low sensitivity of voltage measurement devices to conductivity variations in the region of interest. Image reconstruction in electrical tomography is highly sensitive to modeling inaccuracies arising from poorly characterized auxiliary variables in the measurement model. A common issue is the imperfect knowledge of the object's geometry, with errors in this aspect shown to have significant consequences for the reconstruction process.

In EIT, the solution to the forward problem is to determine the potential distribution in an object, given the boundary conditions and data. The numerical analysis of the problem at this point is presented using the example of electrical impedance tomography and the finite element method. It is currently the most widely used numerical method for the approximate solution of field problems of complex geometry, in which the medium may exhibit characteristics of current heterogeneity, conductivity, etc. Most of the currently used image reconstruction algorithms use this method. Depending on the geometry of the area, there is a tendency to use isoparametric triangular or quadrilateral finite elements.

In medical diagnostics, many methods of imaging the human internal structure are used, each as an independent or complementary method. We should mention here the systems widely used today, with moderate prices, using ultrasound waves (ultrasonography and Doppler apparatus), as well as costly systems (requiring specialized equipment), but providing images (diagnostic information) of very good quality and high resolution, using magnetic resonance imaging (MRI).

Another class of imaging systems uses X-rays (X-ray equipment, computed tomography). Computed tomography (CT – computer tomography) provides us with images of the best quality so far (carrying the most diagnostic information).

The computer tomograph is built based on an X-ray tube with which a sequence of layered images is made. The data set is then subjected to the analytical image reconstruction process. The resulting image, called a tomogram, is obtained and carries information about the distribution of the linear X-ray attenuation coefficient in the examined tissue cross-section. X-ray methods (as opposed to the first two) are harmful to the patient's health, which is particularly important in CT systems, as the patient's absorption dose during a single examination is many times greater than a typical chest X-ray examination.

Impedance measurements appeared in medical research as early as the beginning of the 20th

century and settled permanently in the 1960s. They use the electrical properties of biological tissue (different types of biological tissue (and therefore different organs) and are characterized by different specific impedances [12–15]). The main task of EIT is non-invasive and, at the same time, completely harmless to the patient's health [16–27]. Two-dimensional (or even three-dimensional) imaging of the internal structure of the human body, using the differences above in impedance of the examined structures.

MATERIALS AND METHODS

Measuring system

Figure 1 presents the block diagram of the operation of the impedance tomography system designed for monitoring bladder filling with urine. The control element is an Intel Altera Cyclone IV FPGA, which communicates with the executive components via buses and interfaces. A DAC converter controlled by a functional block in the FPGA system is used as the excitation signal source. This solution allows for generating a signal with any waveform and synchronized phase. Another digital-to-analog converter controls the reference voltage value for the signal source and regulates the signal amplitude. The prepared signal is transmitted to the multiplexer system through a current measurement block (current/voltage converter). Current measurement uses a programmable instrumentation amplifier and an analog-to-digital converter.

Upon detecting the start signal, the system initiates the measurement process, synchronizing the measurement time with a multiple of the signal period duration. This parameter has been implemented as a configurable element to improve measurement accuracy while simultaneously extending the duration of the process itself. The most commonly used value of the measurement time multiplier relative to the excitation signal period is 3, which at an excitation frequency of 50 kHz corresponds to a single measurement duration of 60 μs. This means that each measurement

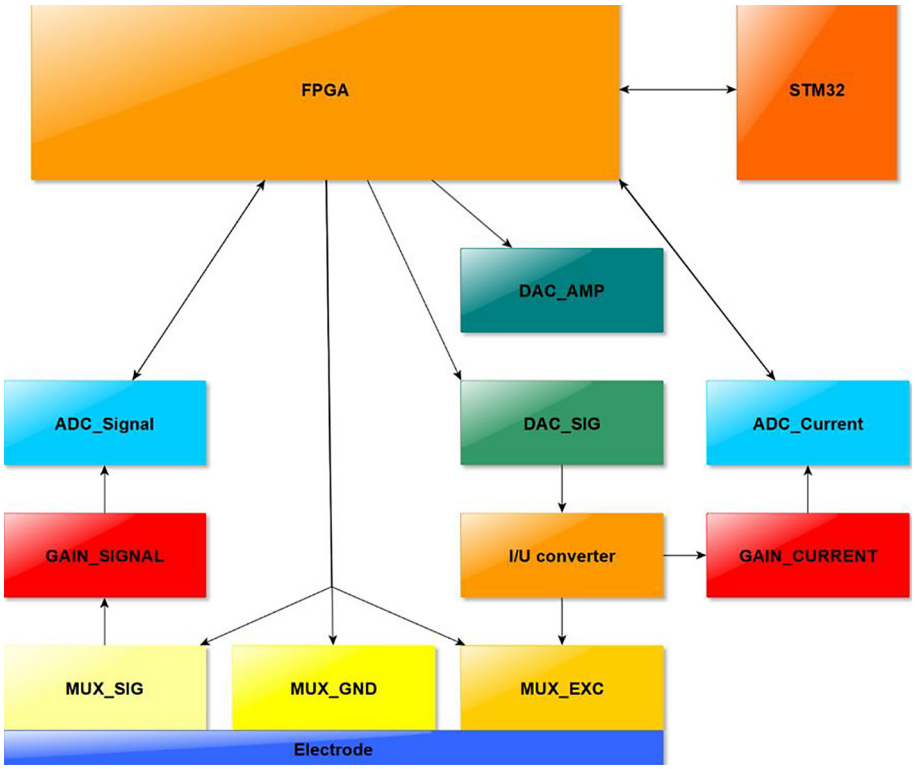

Figure 1. Block diagram of the impedance tomography system designed to monitor bladder filling. The FPGA-based system (Intel Altera Cyclone IV) controls the DAC converter generating the excitation signal, the instrumentation amplifier measuring current and voltage, and the multiplexer switching the measuring electrodes. The analog measurement data is digitized by the ADC converter and sent to RAM, from where it is sent to the data processing unit performing image reconstruction. The arrows indicate the direction of signal flow between the blocks

cycle lasts about 180 µs. Further increasing this value does not bring any noticeable improvement in measurement accuracy.

A single measurement sequence measures both voltage and current values simultaneously. After verifying the correct setting of the current regulation block, the process of recording the measured value to a RAM cell corresponding to the ordinal number of a given measurement in the sequence is initiated in the next clock cycle. Simultaneously, the sequence for switching the multiplexer settings is activated according to the programmed assumptions.

The measurement in the solution is performed cyclically: the signal is measured sequentially on all 16 electrodes, after which the excitation and ground electrode positions are switched to the next in the sequence. The shift between the excitation and ground electrode numbers is executed at the start of the measurement process by setting the initial values of the variables.

The ADC controller block measures current and voltage. This block performs measurement procedures and controls the measurement duration, serving synchronization functions. The number of samples needed to synchronize the process with the signal period correctly is calculated based on the control signal from the excitation signal sources.

The root mean square (RMS) value is measured in two stages. In the first stage, the mean value of the measured signal is calculated, providing information about the DC component of the signal, if present. Next, the absolute values of the measured signals, reduced by the mean value, are summing. In the subsequent clock cycle, the sum is divided by the number of samples, generating a completion flag. This process results in a value proportional to the signal's RMS value.

The FPGA signal measurement and processing system stores one series of measurements in its memory. After completing a cycle of 256 measurements (one series), a readiness flag is set to transfer the data to the processor, where further processing and analysis are performed.

After verifying the correctness and stability of the blocks' operation, tests were conducted to measure the entire matrix. For this purpose, a test probe filled with a saline water solution and a plastic phantom were used (Figure 2).

Five measurement series were recorded for a sequence with an excitation shift relative to the ground by 180°. During the measurements, the measured voltage value and the excitation voltage setting required to achieve the current within the desired range were recorded. The example below sets the acceptable under-regulation range to +/- 1 µA. For this setting, the adequate time for measuring one complete sequence (256 measurements) they are ranged from 50 to 100 ms, corresponding to about 10–20 frames per second. The maximum theoretical measurement speed for these settings, assuming an excitation frequency of 50 kHz and 3 periods per measurement, is 0.016 s, which gives about 60 frames per second. However, this time is extended due to the need for constant current adjustment in real-world objects (Figure 3).

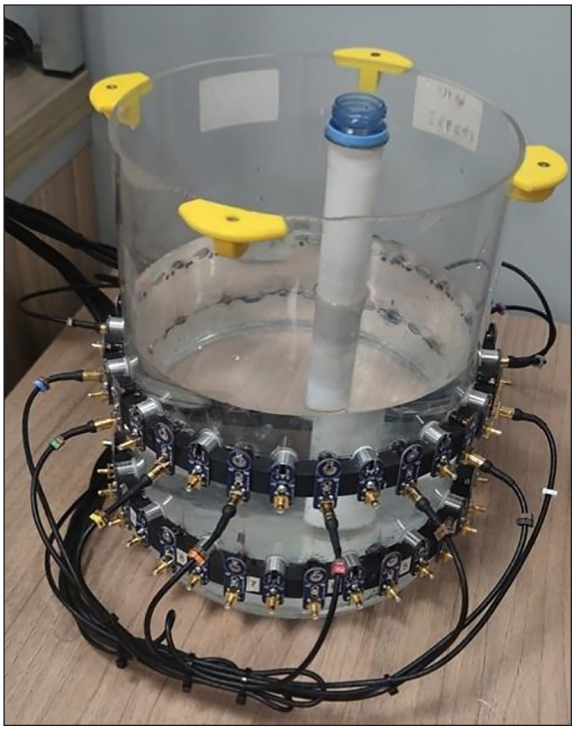

Figure 2. Test tank used for calibration and verification of the EIT device. Inside the tank there is a phantom made of plastic that imitates the conductive properties of biological tissues. On the inner surface of the tank wall, 16 measuring electrodes are placed evenly distributed in one plane. The electrodes are used to cyclically measure voltage and current as part of the measurement sequence. This arrangement allows for simulation of the conditions of a real examination of the urinary bladder using an impedance tomography system

The measuring device is used to image the bladder. The tomography method is based on alternating current stimulation and measuring the voltage on the skin surface. It is possible to reconstruct the studied area from the collected measurements, i.e., to visualize the distribution of

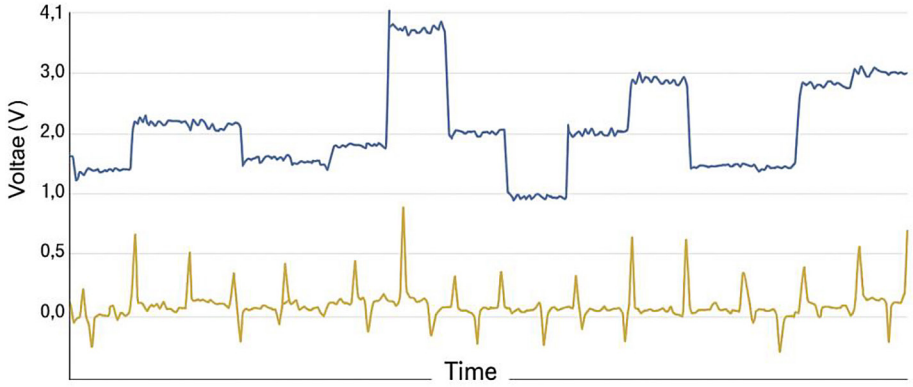

Figure 3. Example of the measurement signal recorded during five measurement series in the test tank. The graph shows the voltage values measured on the electrodes (continuous line) and the corresponding excitation voltage settings (measurement points), which allow maintaining a constant current intensity within the permissible control range of ± 1 μA. The repeatability of the waveforms in subsequent series and the correlation between the excitation voltage and the measurement response of the system are visible. These data are used to assess the stability of the EIT system and the accuracy of the current control

electrical conductivity values. This distribution is obtained using proprietary algorithms primarily based on solving the inverse problem. The transducer module will be fastened to the underwear using a velcro strap (Figure 4) to maintain hygiene and allow for easy device reuse with other patients. Meanwhile, the measurement module is enclosed in a separate box that can be worn on a dedicated belt or placed in another convenient location for the patient. Using the tomography method, the system allows for imaging and monitoring the abdominal cavity in real time.

The device uses an AC excitation sequence between electrodes numbered i and i+3, where i denotes the electrode number in a given electrode strip. There are no excitations between the first and second sets of electrodes. The excitation sequence used allows for collecting 256 measurements. The device records the voltage on the electrodes, the excitation current, the excitation current voltage, and the phase shift of the excitation current. There is dedicated software BETS (bladder electrical tomography system) version 1.1 to operate the device, as shown in Figure 4. The program's functionalities allow for measurement,

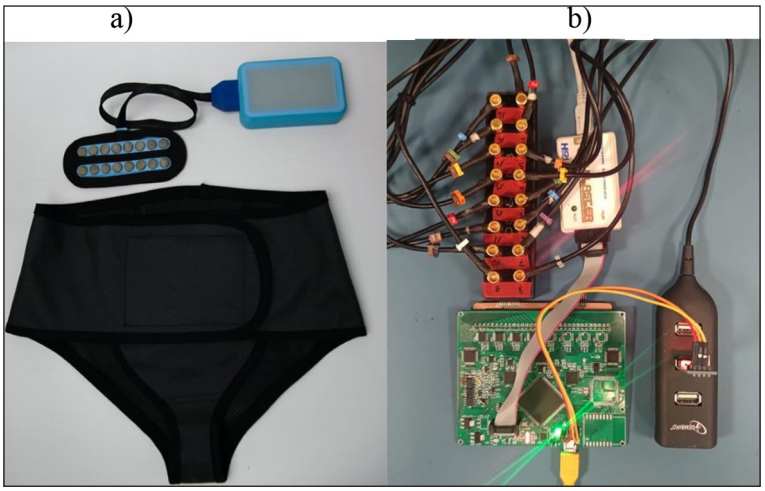

Figure 4. (a) Modular EIT measurement system consisting of the main tomograph module (measuring housing), an electronic unit controlling the measurement procedure (control board), and a set of 16 textile electrodes arranged in two rows of 8, placed in an elastic measuring underwear (visible in the photo); (b) view of the connection of the EIT device to the measuring head using a wire connector. The method of mounting the electrode and the wire leading the measurement signals from the skin surface to the processing unit is shown

visualization, and recording. The desktop application also allows for the reconstruction of a single measurement and a series of measurements, automatically visualized in a graph representing a 2D cross-section of the abdominal cavity. Figure 5 shows the application's user interface.

The device collects voltage measurements and processes them using built-in algorithms to generate a 2D reconstruction. Measurements from one electrode strip were used to perform the presented two-dimensional reconstructions, and the Gauss-Newton method with a regularization constant of 1e-8 was used to solve the inverse problem [28–31]. Additionally, the electrode placement was shown in the reconstruction plots.

Characteristics of electromagnetic compatibility tests

The EMC tests conducted on the device aimed to thoroughly assess its resistance to various electromagnetic disturbances that may occur in its typical operating environment. The tests considered the emission of electromagnetic disturbances and the immunity to such disturbances to ensure the device complies with safety requirements and performance standards for medical devices and home environments. Each test was conducted under controlled laboratory conditions, by established methods and testing protocols, and the results were carefully analyzed against the criteria defined in standards, including PN-EN 55011 and PN-EN 55032.

During the electromagnetic emission tests, both conducted and radiated emissions were examined to assess the device's ability to limit unwanted electromagnetic signals across a wide frequency range. Conducted emissions ranged from 0.15 to 30 MHz, while radiated emissions were measured from 30 MHz to 6 GHz. The results indicate that the device effectively limits electromagnetic emissions to acceptable levels, evidenced by well-designed shielding and filtering components. Meeting these requirements is crucial, as excessive electromagnetic emissions can interfere with the operation of other sensitive devices, especially in medical environments where precise measurements and device stability are essential (Figure 6).

Figure 6 presents merged measurement results obtained for the EUT (equipment under

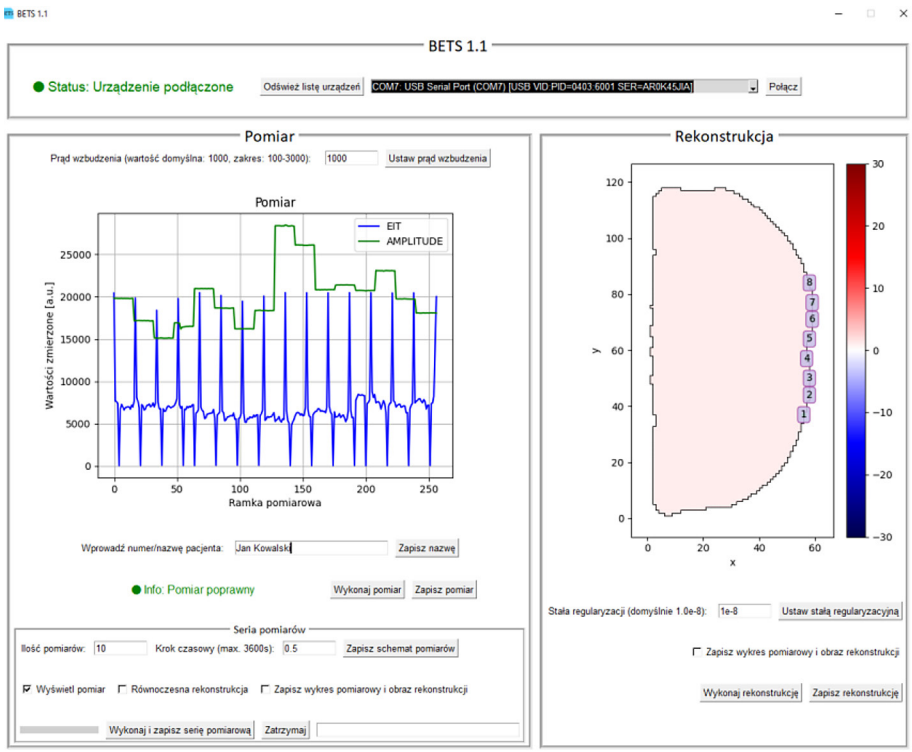

Figure 5. The main panel of the BETS (Bladder Electrical Tomography System) application in version 1.1, used to operate the EIT system. The user interface consists of three main sections: (1) a panel for connecting to a tomographic device via a USB port (with selection of the appropriate COM port), (2) a panel for visualizing measurement signals in real time, and (3) a panel for reconstructing a 2D image showing a cross-section of the abdominal cavity. The program allows for performing, saving, and analyzing single measurements and measurement series with automatic reconstruction of conductivity images

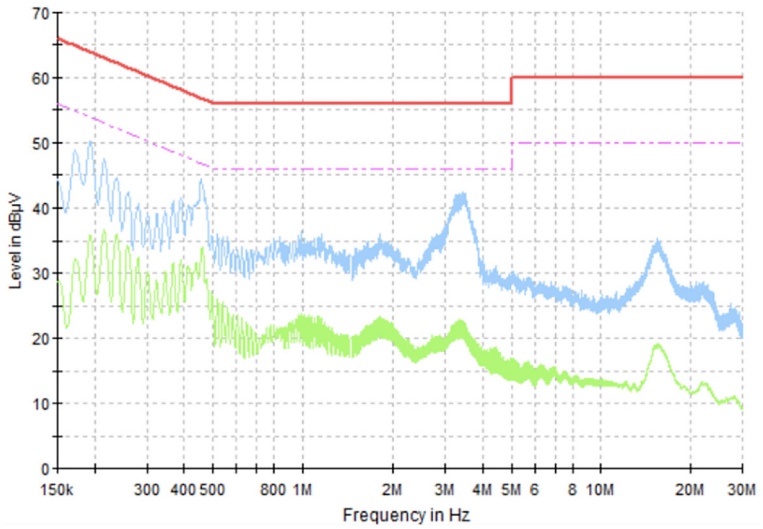

Figure 6. Measurement results of the interference voltages conducted in the power supply port of the device (EUT – Equipment Under Test), obtained during electromagnetic compatibility (EMC) tests. The graph shows the peak values (blue continuous line – peak detector) and average values (green continuous line – average detector) for all measurement frequencies in the range of 0.15–30 MHz. The red line represents the permissible interference level for the quasi-peak detector according to the EN 55011 class B, group 1 standard, and the pink line – for the average detector according to the same standard. The device meets the requirements of the standards in the entire range of tested frequencies

test). This graph includes all measurement results obtained during the preliminary test. Still, it shows only the highest level at each frequency (blue solid line – for peak detector, green solid line – for average detector). Final measurement results for selected frequencies are omitted because recorded levels were more than 10 dB below limits during the preliminary test. The red line is the permissible limit for a qua-si-peak detector by EN 55011 class B group 1 and PN-EN 55032, and the pink line is the allowable limit for the average detector by EN 55011 class B, group 1 and PN-EN 55032.

The immunity tests of the device to electromagnetic disturbances examined the system's response to various external disruptions. The electrostatic discharge (ESD) and electrical fast transient (EFT) immunity tests simulated sudden, short bursts of energy that can occur due to direct user contact with the device or from external electrical disturbances. The device demonstrated a high level of immunity to these disturbances, showing no significant deviations in functionality, confirming its ability to operate stably under real-world conditions. Additionally, surge immunity and power frequency magnetic field tests were conducted to evaluate whether the device can function effectively in strong electromagnetic disturbances, such as fluctuating magnetic fields in typical operational environments (Figures 7–9).

Figure 7 presents merged measurement results obtained for the EUT. This graph includes all measurement results obtained during the preliminary test but shows only the highest level at each frequency (blue line). The final measurement results for selected frequencies are presented as blue rhombus (using a quasi-peak detector). The red line is the permissible limit for EN 55011 class B, group 1 devices, PN-EN 55032, and QP detectors. In the case of the radiated emission test (Figure 7), local exceedances of the permissible interference levels for class B according to the EN 55011 standard were observed. These exceedances occurred in a narrow frequency range and were repeatable in subsequent tests. They were most likely caused by conductive elements inside the housing not covered by sufficient shielding. Therefore, design modifications to the device are planned (including strengthening the shielding and signal filtering), which will be taken into account before the product is implemented in clinical practice. Despite the exceedances, the device demonstrated stable operation without loss of functionality, which is also confirmed by interference immunity tests.

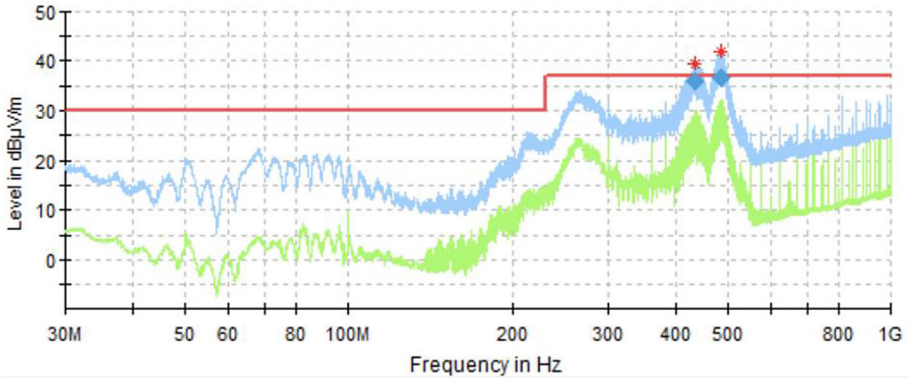

Figure 7. Results of the measurement of the level of radiated interference emitted by the EUT (equipment under test) in the frequency range of 30 MHz – 1 GHz, performed during electromagnetic compatibility (EMC) tests. The blue line shows the highest recorded signal level in a given frequency during the preliminary test. The blue diamonds indicate the final measurement values obtained with the quasi-peak (QP) detector. The red line shows the permissible emission level according to the EN 55011 class B, group 1 standard. Local exceedances of the limit values are visible in several frequency ranges, which is discussed in the body of the article

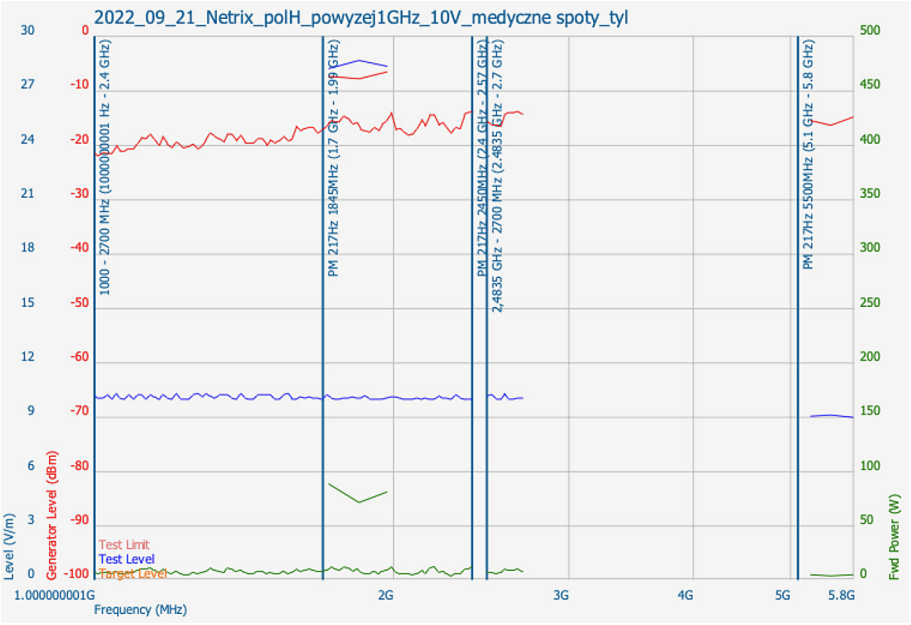

Figure 8. Electromagnetic field levels recorded during a radiation immunity test in the 1 GHz – 2.7 GHz range using horizontal polarization, conducted in an anechoic chamber (SAC). The blue line shows the level of electric field exposure (E-field) in the vicinity of the tested device (EUT - equipment under test). The test was performed in accordance with the PN-EN 61000-4-3 standard. The device did not show any interference in operation, which confirms its immunity to radiated interference in this frequency band

As part of the electromagnetic radiation immunity tests, measurements were carried out in the SAC (Semi-Anechoic Chamber), in the frequency range from 1 GHz to 2.7 GHz. Figure 8 shows the levels of exposure to the electromagnetic field (horizontal polarization), recorded in the vicinity of the tested device (EUT). All recorded values were below the permissible thresholds specified in the PN-EN 61000-4-3 standards, which confirms the device's immunity to interference in this frequency band.

The radiation immunity tests in the 1–2.7 GHz band are supplemented by measurements performed using vertical polarization, the results of which are shown in Figure 9. As in the case of horizontal polarization, all recorded exposure values were below the permissible thresholds according to the PN-EN 61000-4-3 standard.

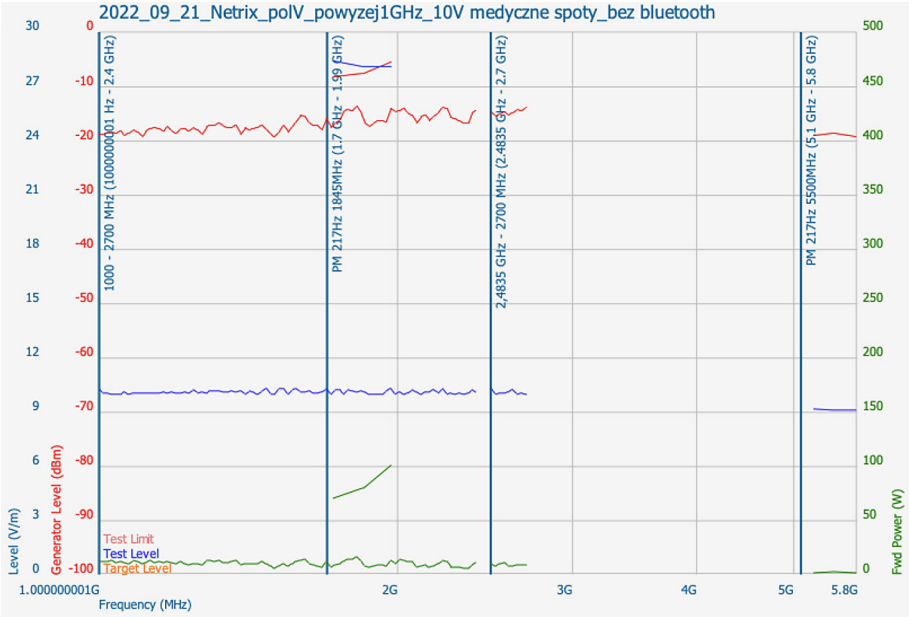

Figure 9. Electromagnetic field levels recorded during a radiation immunity test in the 1 GHz – 2.7 GHz frequency range, conducted in a semi-anechoic chamber (SAC) using vertical polarization. The blue line shows the electric field (E-field) exposure level in the vicinity of the EUT (Equipment Under Test). The device met the interference immunity criteria according to the PN-EN 61000-4-3 standard, showing no functional interference

The device did not show any undesirable reactions, which confirms its immunity also in this measurement system.

The conducted EMC tests confirmed that the device meets stringent electromagnetic compatibility requirements, both in terms of minimizing emissions and in terms of immunity to external disturbances. This ensures that the device can be safely used in medical environments, where operational stability and reliability are crucial, as well as in home environments. The results obtained during the tests comply with the standard requirements, providing a basis for a positive assessment of the device's compliance and further certification. These tests represent an important stage in the evaluation and market introduction of medical devices, ensuring their safety, performance, and reliability across a wide range of applications.

RESULTS

A machine learning model was applied to receive an image reconstruction from the obtained EIT measurements. In the context of energy and time optimization, it is important to choose the proper reconstruction method. In this section, three different machine learning algorithms were presented and compared: Decision Tree, NNET, and Elastic Net. The application of artificial intelligence provides a non-invasive and effective solution for the image reconstruction problem.

The models were trained on EIT simulated data using R programming language [32] and packages such as rpart (version 4.1.19) [33], nnet (version 7.3.18) [34], and glmnet (version 4.1.7) [35]. The Electrical Tomography Impedance (EIT) dataset was generated by simulation based on realistic anatomical models representing the conduction conditions in the lower abdominal cavity. The training set consisted of a measurement matrix (3750 observations of the measurement vector) and corresponding image data of the urinary bladder (3750 observations of 7320 pixels). The measurement vector contained 32 voltage measurements at the measuring electrodes. The adopted measurement sequence was intended to reflect the designed hardware. The test set consisted of 1250 observations. A model was built for each of the 7320 pixels. This approach ensures better reconstruction quality. It was applied for every discussed method. Due to the number of models being built, the hyperparameters were selected by manual search. The paper contains exemplary image reconstructions and the comparison of the models using measures such as mean squared error (MSE, formula 1) and structural similarity index (SSIM, formula 2).

$$MSE = \frac{1}{n}\sum_{i=1}^{n}(x_i - y_i)^2 \quad (1)$$

where: x_i is the true value, y_i denotes the predicted value and n is the sample size.

$$SSIM = \frac{(2\mu_x\mu_y + c_1)(2\sigma_{xy} + c_2)}{(\mu_1^2 + \mu_2^2 + c_1)(\sigma_1^2 + \sigma_2^2 + c_2)} \quad (2)$$

where: c_1 and c_2 balance the division, μ_x, μ_y are the mean values of x and y, σ_1^2, σ_2^2 are the variances of x and y, σ_{xy} is the covariance of x and y.

The metrics were calculated for each case and then averaged. The selection of algorithms for image reconstruction from EIT measurements was guided by the need to balance three fundamental criteria: prediction accuracy, computational efficiency, and feasibility of application in real-time systems. Given the inherent limitations of EIT, including the relatively low spatial resolution and the nonlinearity of electrical current propagation in biological tissues, it is crucial to employ machine learning techniques that are capable of modeling complex relationships between voltage measurements and the corresponding internal conductivity distribution while maintaining acceptable processing times. The first method analysed was the Decision Tree, a model that partitions the input space into hierarchically structured regions based on sequential decision rules [36]. Decision trees are valued for their transparency and intuitive interpretability, making them suitable for scenarios where model explainability is critical. While relatively fast and straightforward to implement, they are prone to overfitting, especially in the absence of appropriate pruning mechanisms. Despite this, their ability to model non-linear relationships makes them a relevant baseline in the context of EIT. The second approach, neural network (NNET), utilizes layers of interconnected artificial neurons to approximate complex functions [37]. In the context of EIT, neural networks are particularly advantageous due to their capacity to learn intricate, non-linear mappings from measurement data to reconstructed images. Proper configuration of the network architecture and training parameters allows for effective generalization and robust performance. When adequately regularized and trained, neural networks can offer both high reconstruction accuracy and low latency, making them promising candidates for deployment in energy- and time-constrained systems. The third method, Elastic Net, represents a linear regression model enhanced with a combination of L1 and L2 regularization [38]. This hybrid penalty framework allows the model to handle high-dimensional data and multicollinearity more effectively than traditional regression methods. Elastic Net is particularly suitable when the number of predictors is large relative to the number of observations. However, as a linear model, it may be less capable of capturing the complex, non-linear structures typically present in EIT data, which can limit its reconstruction accuracy in comparison to more flexible models. The three selected algorithms reflect a range of modelling philosophies—from simple to complex. This diversity enables a comprehensive assessment of their respective strengths and limitations in the context of EIT-based image reconstruction, with a particular focus on balancing accuracy, computational demand, and practical applicability.

Comparison of machine learning algorithms

Three machine learning algorithms were compared in the context of reconstructing images from EIT measurements: decision tree, NNET, and elastic net. A decision tree is a machine learning model that facilitates data classification or regression by organizing information into a hierarchical structure of conditions. The algorithm recursively partitions the dataset into progressively smaller subsets, ultimately reaching terminal nodes, or "leaves," which correspond to the final predictions for individual observations. The partitioning process at each node is guided by criteria such as entropy, the Gini index, or mean squared error, depending on the task at hand. While decision trees are intuitive and easily interpretable, they are prone to overfitting, particularly when the tree structure becomes overly complex or too deep. To mitigate overfitting, various techniques such as pruning, cross-validation, or tree aggregation methods—like random forests or boosting—are employed. Decision trees are versatile models suitable for a range of applications, including forecasting, data mining, dimensionality reduction, and detecting interactions between variables (Figure 10).

The NNET model is a neural network available through the nnet package in R, commonly used for machine learning tasks that require uncovering complex patterns and relationships in data. A neural network is composed of layers of artificial neurons, where each neuron processes input data via activation functions and weighted

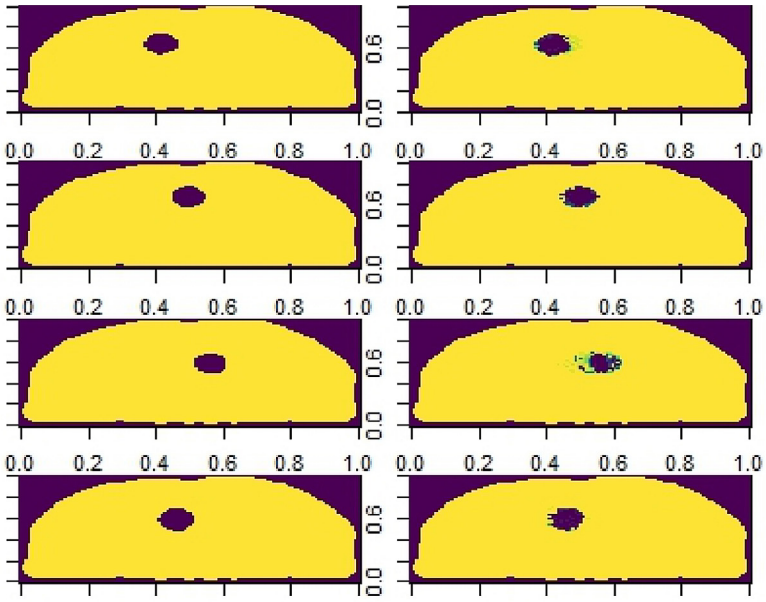

Figure 10. Comparison of the original object (on the left) and the Decision Tree reconstruction (on the right) for four randomly selected cases from the test set

connections. The nnet package allows the creation and training of a feedforward neural network with a single hidden layer. The model can be applied to both classification and regression tasks, depending on the nature of the target variable – either categorical or numeric. It is trained using a backpropagation algorithm, which fine-tunes the network's weights by minimizing the errors between predicted and actual outcomes. Additionally, regularization is used to prevent overfitting by penalizing excessively large weights. In this configuration, the model uses three neurons in the hidden layer, balancing the ability to capture intricate patterns with the risk of overfitting. The weights are initialized randomly within a specified range of 0.2, influencing the initial state of the network's learning. To prevent overfitting, a small regularization factor (0.0005) is applied, which improves generalization by adding a penalty to large weights. The learning algorithm is set to run for a maximum of

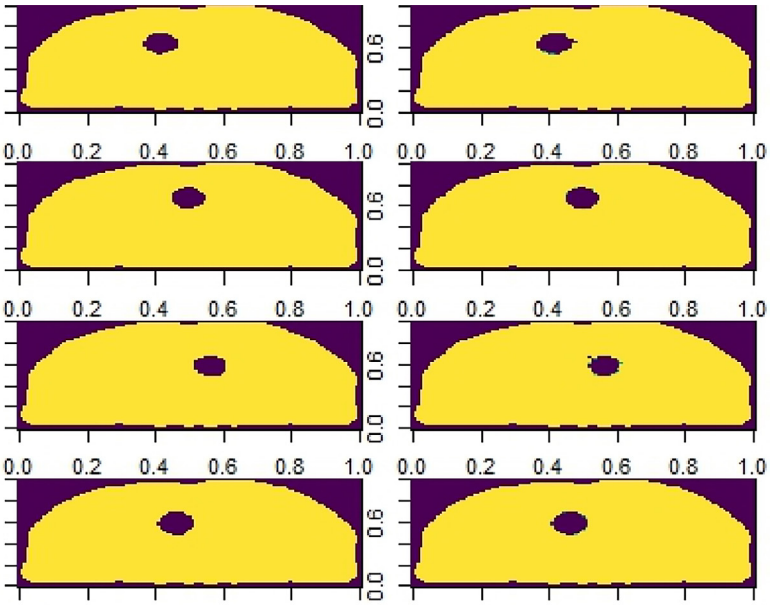

Figure 11. Comparison of the original object (on the left) and the NNET reconstruction (on the right) for four randomly selected cases from the test set

200 iterations, allowing sufficient exploration of the solution space, though extended training can increase the risk of getting stuck in local minima and lengthen the computation time. This configuration enables the model to learn effectively while managing the trade-off between complexity and overfitting (Figure 11).

The Elastic Net is a linear regression model that incorporates both L1 and L2 penalties as a form of regularization, effectively combining the strengths of Ridge and Lasso regression. This dual regularization method helps reduce dimensionality and prevents overfitting, making it particularly useful when the dataset contains a large number of features compared to the number of observations. By applying regularization, Elastic Net ensures that the model remains generalizable, even in high-dimensional spaces. The degree to which the L1 and L2 penalties are applied is controlled by the alpha parameter, which ranges from 0 to 1. When alpha equals 0, the model behaves as Ridge regression (L2 penalty), and when alpha equals 1, it mimics Lasso regression (L1 penalty). For values of alpha between 0 and 1, Elastic Net applies a combination of both penalties, allowing for greater flexibility in controlling the model's complexity. Elastic Net is widely employed in fields such as data analysis, text mining, and visualization, where it excels in handling datasets with many correlated variables. Its ability to manage the problem of multidimensionality, particularly when the number of variables exceeds the number of observations, makes it a robust choice for regression tasks that require balancing bias and variance (Figure 12).

Image reconstruction quality

Table 1 compares the performance of three discussed machine learning algorithms based on two metrics: MSE (mean squared error) and SSIM (structural similarity index). The lower the value of MSE and the higher the value of SSIM, the better the quality of the obtained image reconstructions. Additionally, the time of prediction generation was measured. Regarding energy and performance optimization, the model should have the most minor reconstruction error and make predictions in the shortest time possible. It can be seen that the NNET method (a neural network with 3 neurons in the hidden layer) has the lowest MSE and the highest SSIM, what suggests that it has the best forecasting quality. It also makes predictions in the shortest time of 7.49 seconds. The Decision Tree algorithm has slightly higher MSE value than the NNET model, what means that it is less efficient at predicting the value of the dependent variable. The Elastic Net algorithm has the highest MSE value, indicating the worst forecasting accuracy. However, from the prediction time point of view, it performs similarly to the NNET network. Among the evaluated methods, the NNET one proved to be

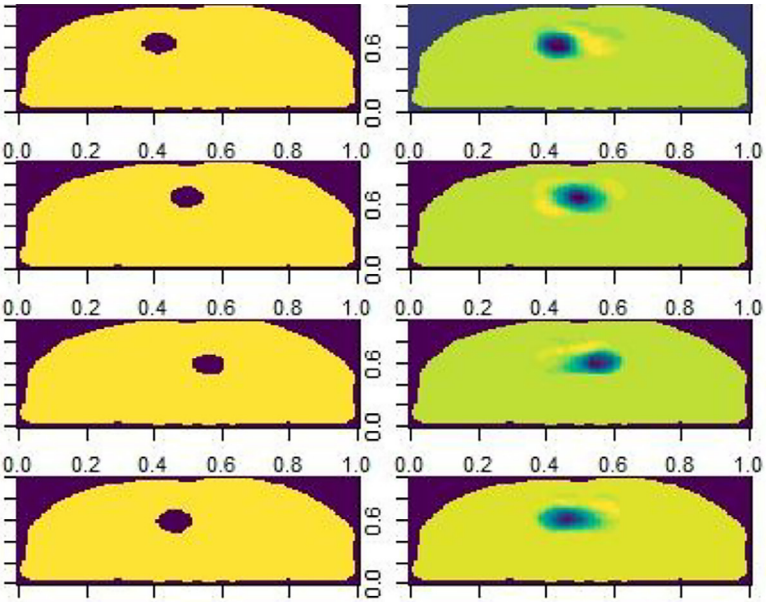

Figure 12. Comparison of the original object (on the left) and the Elastic Net reconstruction (on the right) for four randomly selected cases from the test set

Table 1. Comparison of image reconstruction indicators

The method	Time [s]	Indicator	
		MSE	SSIM
Decision tree	25.96	0.002255	0.999969
NNET	7.49	0.0004245	0.9999945
Elastic net	8.47	0.004616	0.9999368

the most effective for EIT-based image reconstruction. It offers the best balance between accuracy and computational efficiency, making it a suitable choice for energy-aware and real-time applications. Despite its numerous advantages, EIT has several significant limitations that can affect the quality of the obtained results. One of the key challenges is its sensitivity to modelling errors. Small inaccuracies in the geometric model of the examined object or errors in the assumptions regarding conductivity properties can significantly reduce the quality of image reconstruction. In addition, the limited number of available measurements and the nonlinear nature of current flow through various media inside the body make it difficult to obtain high-resolution images. Another significant limitation is the imperfection of the measurement equipment, especially the sensitivity of the sensors and limitations in the precision of voltage and current measurements. Even small disturbances in the electrical contacts between the electrodes and the patient's skin can lead to errors in the measurement results, which in turn affects the quality of image reconstruction. In the case of portable EIT devices, where compact and energy-efficient solutions are required, limitations related to the miniaturization of the equipment can also affect the accuracy of the obtained images. Despite the promising results obtained using image reconstruction algorithms in EIT, this technique is still limited by its sensitivity to modelling errors and hardware imperfections. Future research will need to focus on improving measurement accuracy, developing more advanced mathematical models, and designing more efficient sensors. These improvements will allow for increased precision in image reconstruction and broader applications of EIT in medical diagnostics. To summarize the research, the most suitable method is the NNET neural network. It provides fast and high-quality prediction. Artificial intelligence is an appropriate and beneficial solution to the image reconstruction problem based on EIT measurements.

CONCLUSIONS

The EIT enables non-invasive study of internal processes in objects, without the need for direct intervention. The collected data is analysed and transformed into images using specialized algorithms. However, this form of tomography suffers from limitations in image resolution. Challenges include the limited number of measurements, the complex nature of electric currents in different media, and the low sensitivity of voltage measurements to conductivity changes in the studied area. A key challenge remains the development of precise measurement tools and algorithms for effective image reconstruction. Data analysis plays a key role in tomography-based diagnostics, and the inverse problem is related to optimization, identification, or synthesis, where parameters describing the field are inferred from the collected information. These problems are complex, often lack clear solutions, and are prone to misinterpretation due to insufficient or excessive data. A better understanding of the reconstruction process can increase the system's robustness to incomplete data. Our research has shown that in processes based on electrical tomography, there is no single, universal method that is ideal for data reconstruction and analysis. Machine learning methods, such as Elastic Net, may be less precise with real measurement data, but they offer relatively fast results. In the context of optimization, the NNET neural network turned out to be the most effective solution. The research results were presented both graphically and numerically, which facilitates visual and quantitative analysis of the results. The developed algorithms and observations can be used in various medical fields, which opens the way to new clinical applications. According to the results of our research, special attention should be paid to the further development of image reconstruction techniques, including the use of more advanced deep learning methods. Potentially, the combination of impedance tomography techniques with ultrasound can significantly increase the precision of diagnosing and monitoring internal organ dysfunctions, especially in the field of pediatric medicine. However, it is worth noting that achieving high resolution requires not only improving algorithms, but also optimizing measurement systems, including improving sensors and developing new signal processing methods.

Our research confirms the growing importance of artificial intelligence applications in medical imaging techniques. While previous studies focused mainly on classical reconstruction methods, our work introduces new perspectives related to the use of methods such as neural networks and their advantages over other techniques in specific conditions [1]. Our results are consistent with this trend, and at the same time indicate the need for further work on the development of more advanced models.

Practical applications of this technology include not only medical diagnostics, but also monitoring and control of technological processes in industry. In particular, the integration of EIT technology with remote monitoring systems could be a significant step forward in such fields as biomedical engineering, process control or construction. The key direction of future research should be not only improving the reconstruction methods, but also analysing the energy efficiency of these systems, which is of particular importance for portable and wearable devices.

Our research highlights the potential of EIT techniques supported by machine learning in medical imaging and diagnostics. Future research should focus on further optimization of algorithms, as well as integration of different imaging techniques to maximize their precision and efficiency. This technology also has wide application possibilities in other industries, including monitoring industrial processes and developing remote diagnostic systems.

REFERENCES

1. Kłosowski, G., Hoła, A., Rymarczyk, T., Mazurek, M., Niderla, K., Rzemieniak, M. Use of the double-stage LSTM network in electrical tomography for 3D wall moisture imaging. Measurement 2023, 213, 1–13, https://doi.org/10.1016/j.measurement.2023.112741
2. Kłosowski, G., Hoła, A., Rymarczyk, T., Mazurek, M., Niderla, K., Rzemieniak, M. Using machine learning in electrical tomography for building energy efficiency through moisture detection. Energies 2023, 16, 1818. https://doi.org/10.3390/en16041818
3. Rymarczyk, T., Mazurek, M., Hyka, O., Wójcik, D., Dziadosz, M., Kowalski, M. Poster Abstract: A Wearable for Non-Invasive Monitoring and Diagnosing Functional Disorders of the Lower Urinary Tract. Conference: SenSys '23: 21st ACM Conference on Embedded Networked Sensor Systems 2023, https://doi.org/10.1145/3625687.3628382
4. Baran, B., Kozłowski, E., Majerek, D., Rymarczyk, T., Soleimani, M., Wójcik, D. Application of machine learning algorithms to the discretization problem in wearable electrical tomography imaging for bladder tracking. Sensors 2023, 23, 1553. https://doi.org/10.3390/s23031553
5. Przysucha, B., Wójcik, D., Rymarczyk, T., Król, K., Kozłowski, E., Gąsior, M. Analysis of reconstruction energy efficiency in EIT and ECT 3D tomography based on elastic net. Energies 2023, 16, 1490. https://doi.org/10.3390/en16031490
6. Wójcik, D., Rymarczyk, T., Przysucha, B., Gołąbek, M., Majerek, D., Warowny, T., Soleimani, M. Energy reduction with super-resolution convolutional neural network for ultrasound tomography. Energies 2023, 16, 1387. https://doi.org/10.3390/en16031387
7. Kłosowski, G., Rymarczyk, T., Niderla, K., Kulisz, M., Skowron, Ł., Soleimani, M. Using an LSTM network to monitor industrial reactors using electrical capacitance and impedance tomography – a hybrid approach. Eksploatacja i Niezawodność – Maintenance and Reliability 2023, 25, 1–11. https://doi.org/10.17531/EIN.2023.1.11
8. Kozłowski, E., Borucka, A., Oleszczuk, P., Jałowiec, T. Evaluation of the maintenance system readiness using the semi-Markov model taking into account hidden factors. Eksploatacja i Niezawodność – Maintenance and Reliability 2023, 25, 1–17. https://doi.org/10.17531/ein/172857
9. Dziadosz, M., Bednarczuk, P., Pietrzyk, R., Sutryk, M. Advanced bladder analysis using ultrasonic and electrical impedance tomography with machine learning algorithms. Journal of Modern Science 2024, 57, 637–651, https://doi.org/10.13166/jms/191360.
10. Król, K., Rymarczyk, T., Niderla, K., Kozłowski, E. Sensor platform of industrial tomography for diagnostics and control of technological processes. Informatyka, Automatyka, Pomiary w Gospodarce i Ochronie Środowiska 2023, 13, 33–37. https://doi.org/10.35784/iapgos.3371
11. Kłosowski, G., Rymarczyk, T. Application of convolutional neural networks in wall moisture identification by eit method. Informatyka, Automatyka, Pomiary w Gospodarce i Ochronie Środowiska 2022, 12, 20-23. https://doi.org/10.35784/iapgos.2883
12. Holder, D.S. Electrical Impedance Tomography: Methods, History and Applications, CRC Press: Boca Raton, FL, USA, 2004.
13. Bayford, R.H. Bioimpedance tomography (electrical impedance tomography). Annu. Rev. Biomed. Eng. 2006, 8, 63–91.
14. Hafid A., Difallah S., Alves C., et al. State of the art of non-invasive technologies for bladder monitoring: a scoping review. Sensors 2023, 23(5), 2758.

https://doi.org/10.3390/s23052758

15. Krawczyk, A., Korzeniewska, E. Some aspects of electromagnetic field shielding. Przegląd Elektrotechniczny 2023, 99, 128-131. https://doi.org/10.15199/48.2023.03.22
16. Holder, D. Introduction to Biomedical Electrical Impedance Tomography Electrical Impedance Tomography Methods, History and Applications, Institute of Physics: Bristol, UK, 2005.
17. Dziadosz, M., Mazurek, M., Stefaniak, B., Wójcik, D., Gauda, K. A comparative study of selected machine learning algorithms for electrical impedance tomography. Przegląd Elektrotechniczny 2024, 1(4), 239–242. https://doi.org/10.15199/48.2024.04.47
18. Rymarczyk, T., Adamkiewicz, P., Duda, K., Szumowski, J., Sikora, J. New electrical tomographic method to determine dampness in historical buildings. Arch. Electr. Eng. 2016, 65, 273–283.
19. Karhunen, K., Seppänen, A., Kaipio, J.P. Adaptive meshing approach to identification of cracks with electrical impedance tomography. Inverse Probl. Imaging 2014, 8, 127–148.
20. Shu, X., Zhang, S., Li, Y., Chen, M. An anomaly detection method based on random convolutional kernel and isolation forest for equipment state monitoring. Eksploatacja i Niezawodność – Maintenance and Reliability 2022, 24, 758–770. https://doi.org/10.17531/EIN.2022.4.16
21. Kryszyn, J., Wanta, D., Smolik, W. Gain adjustment for signal-to-noise ratio improvement in electrical capacitance tomography system EVT4. IEEE Sens. J. 2017, 17, 8107–8116.
22. Al Hosani, E., Soleimani, M. Multiphase permittivity imaging using absolute value electrical capacitance tomography data and a level set algorithm. Philos. Trans. R. Soc. A 2016, 374, 20150332.
23. Pawlik, P., Kania, K., Przysucha, B. Fault diagnosis of machines operating in variable conditions using artificial neural network not requiring training data from a faulty machine. Eksploatacja i Niezawodność – Maintenance and Reliability 2023, 25, 1–14, https://doi.org/10.17531/EIN/168109
24. Gałązka-Czarnecka, I., Korzeniewska, E., Czarnecki, A., Stańdo, J. Modification of color in turmeric rhizomes (Curcuma longa L.) with pulsed electric field. Przegląd Elektrotechniczny 2023, 99, 123–125. https://doi.org/10.15199/48.2023.06.24
25. Majchrowicz, M., Kapusta, P., Jackowska-Strumiłło, L., Sankowski, D. Acceleration of image reconstruction process in the electrical capacitance tomography 3D in heterogeneous, multi-GPU system. Inform. Control Meas. Econ. Environ. Prot. 2017, 7, 37–41.
26. Banasiak, R., Wajman, R., Jaworski, T., Fiderek, P., Fidos, H., Nowakowski, J., Sankowski, D. Study on two-phase flow regime visualisation and identification using 3D electrical capacitance tomography and fuzzy-logic classification. Int. J. Multiph. Flow 2014, 58, 1–14.
27. Rybak, G., Strzecha, K. Short-time Fourier transform based on metaprogramming and the stockham optimization method, Sensors 2021, 21(12), 4123, https://doi.org/10.3390/s21124123
28. Rząsa, M. R. Selection of optical tomography parameters for gas bubble shape analysis. Chemical and Process Engineering, 2014, 35(1), 19–33. https://doi.org/10.2478/cpe-2014-0002
29. Rząsa, M.R. The measuring method for tests of horizontal two-phase gas–liquid flows, using optical and capacitance tomography. Nucl. Eng. Des., 2009, 239, 699–707. https://doi.org/10.1016/j.nucengdes.2008.12.020
30. Strzecha, K., Rybak, G. Automatic evaluation algorithms for radio tomography imaging methods. Sensors, 2025, 25(6), 1747. https://doi.org/10.3390/s25061747
31. Rybak, G., Strzecha, K., Krakós, M. (2022). A new digital platform for collecting measurement data from the novel imaging sensors in urology. *Sensors*, *22*(4), 1539. https://doi.org/10.3390/s22041539
32. R Core Team. (n.d.). *R: A language and environment for statistical computing*. R Foundation for Statistical Computing. https://www.r-project.org/ (accessed on 28 May 2025).
33. Therneau, T., Atkinson, B. (n.d.). *rpart: Recursive Partitioning and Regression Trees (Version 4.1.19)* [R package]. RDocumentation. https://www.rdocumentation.org/packages/rpart/versions/4.1.19 (accessed on 28 May 2025).
34. Venables, W. N., Ripley, B. D. (n.d.). *nnet: Feed-Forward Neural Networks and Multinomial Log-Linear Models (Version 7.3-18)* [R package]. RDocumentation. https://www.rdocumentation.org/packages/nnet/versions/7.3-18 (accessed on 28 May 2025).
35. Friedman, J., Hastie, T., & Tibshirani, R. (n.d.). *glmnet: Lasso and Elastic-Net Regularized Generalized Linear Models (Version 4.1-7)* [R package]. RDocumentation. https://www.rdocumentation.org/packages/glmnet/versions/4.1-7 (accessed on 28 May 2025).
36. Mienye, D., Jere, N. A Survey of Decision Trees: Concepts, Algorithms, and Applications. IEEE Access 2024. PP. 1-1. 10.1109/ACCESS.2024.3416838.
37. Qamar, R., Zardari, B. Artificial Neural Networks: An Overview. Mesopotamian Journal of Computer Science 2023. 130-139. 10.58496/MJCSC/2023/015.
38. Chamlal, H., Benzmane, A., Ouaderhman, T. Elastic net-based high dimensional data selection for regression. Expert Systems with Applications 2024. 244. https://doi.org/10.1016/j.eswa.2023.122958